RESEARCH ARTICLE OPEN ACCESS

Single-Cell Analysis Integrated With Machine Learning Elucidates the Mechanisms of Nucleus Pulposus Cells Apoptosis in Intervertebral Disc Degeneration and Therapeutic Interventions

Chao Song[1,2] 🆔 | Xiaofei Wu[1] | Chaoqi Chen[1] | Baoxin Shen[1] | Yongliang Mei[2] | Qian Yan[1] | Feng Jiang[2] | Feng Chen[1] | Fei Liu[1,2]

[1]Department of Orthopedics, RuiKang Hospital Affiliated to Guangxi University of Chinese Medicine, Nanning, China | [2]Department of Orthopedics and Traumatology, the Affiliated Traditional Chinese Medicine Hospital, Southwest Medical University, Luzhou, China

Correspondence: Feng Chen (chenf1986@gxtcmu.edu.cn) | Fei Liu (lfxnykd@163.com)

ABSTRACT

Background: The molecular of intervertebral disc degeneration (IVDD) is still unclear. When it comes to treating decoction, traditional Chinese medicine is effective. In particular, the Duhuo (Radix Angelicae Biseratae) may be particularly helpful.

Purpose: To identify nucleus pulposus cells (NPCs) subpopulations and immune cells and clarify the mechanism of IVDD therapy, offering recommendations for diagnosis and treatment.

Methods: IVDD targets from the Genecards and microarray data from biological databases. To find the key genes and biological pathways underlying IVDD, multiple machine learning techniques were used. IVDD is associated with subpopulations of NPCs as revealed by single-cell analysis, and immunological infiltration was identified by Immune Cell AI. To validate the molecular pathways by which Duhuo activity affects IVDD, network pharmacology and molecular docking were employed.

Results: The process of IVDD is linked to key genes like TP53, JUN, PTEN, IL1B, ERBB2, MAPK8, CASP9, PTK2, etc. The main molecular mechanisms involved in this process are immune responses, inflammatory factors expression, cellular responses to mechanical stimuli, and NPC apoptosis. Immune Cell AI discovered a correlation between CD4 naïve, B cell, monocyte, NK, and macrophage infiltration with the development of IVDD. The NPC subtypes associated with IVDD, namely fibroNPCs, adhesion NPCs, regulatory NPCs, homeostatic NPCs, and hypertrophic chondrocyte-like NPCs (HT-CL NPCs), were the subject of single-cell mapping. We also found that Osthole, Columbianadin, and Bergapten, the principal blood entry components of Dohuo, may have a role by modulating CASP9, MAPK8, PTGS1, and PARP1, the targets of apoptosis.

Conclusion: The NPC subpopulations that exist in IVDD are HT-CL NPCs, fibroNPCs, adhesion NPCs, regulatory NPCs, and homeostatic NPCs. Furthermore, a variety of immune cell infiltrates, particularly monocyte and macrophage, have a significant

---

Chao Song and Xiaofei Wu contribution equally to this work.

impact on the advancement of IVDD. Osthole, Columbianadin, and Bergapten, the principal components of Duhuo, absorb IVDD via controlling the death of NPCs.

1 | Introduction

The incidence of degenerative diseases is rising annually due to population aging, having a major negative impact on the physical health of the elderly, and is currently garnering increased attention [1]. The spine is the most important structure in the human body. It supports the entire body while bearing the majority of its weight, and as we age, it experiences the most severe degradation [2]. The most typical of these is called intervertebral disc degeneration, or IVDD. More than 90% of adults over 50 years are estimated to have IVDD by statistics [3]. One of the main causes of low back pain (LBP), which has a significant impact on patients' chances of survival, is IVDD [4, 5]. The core gelatinous nucleus pulposus (NP), the peripheral annulus fibrosus (AF), and the cartilaginous endplate (CEP) make up the majority of the intervertebral disc (IVD) [6, 7]. Owing to its unique structure, which gives the spine its compressive, tensile, and flexible properties, NP is essential to the preservation of spinal morphology and function [8]. Consequently, it is critical to research NP's mode of action in IVDD [6].

IVDD development is closely linked to aging, genetics, mechanical loading, malnourishment, immune-inflammatory response, and NP cells (NPCs) death. Degradation and mineralization of the extracellular matrix (ECM), inflammatory responses, and apoptosis are among its main pathological features [9, 10]. With increased degeneration and pain onset, cells in the IVD emit pro-inflammatory cytokines, notably TNF-α, IL-1β, and IL-6, which further promote ECM degradation and apoptosis, as well as trigger the immunological response, resulting in immune cell and nerve fiber infiltration [11, 12]. The evidence supporting the notion that apoptosis is a significant kind of cell death in IVD and that it is essential to disc degeneration has grown recently [13]. Loss of cells due to unchecked or excessive apoptosis can be harmful to one's health. When NPCs undergo excessive apoptosis, the density of NPCs in disc tissue decreases, impairing disc structure and function and resulting in IVDD [14]. It was discovered that berberine inhibits the NF-κB pathway, shielding human NPCs from IL-1β-induced ECM breakdown and death [15]. As a result, it is critical to prevent IVDD from NPC apoptosis because it is a major factor in IVDD.

Physical therapy and medication therapy are now the two main therapeutic modalities for IVDD. According to the group's initial research, IVDD can be effectively treated with Dohuo Jisheng Decoction (DHJSD). The traditional formula for treating IVDD is DHJSD, which has the benefits of nourishing the kidneys and liver, enhancing blood and qi, eliminating wind-dampness, eliminating excruciating pain, and eliminating wind-dampness [16]. Recent research in pharmacology has shown that DHJSD possesses immunomodulatory and anti-inflammatory properties. Through the SDF1/CXCR4-NF-kB pathway, we have previously discovered that DHJSD can suppress the inflammatory expression of human degenerative NPCs in vitro. Furthermore, research recently published demonstrated that DHJSD, when used to treat IVDD, suppresses NPC pyroptosis via the SDF1/ CXCR4-NFkB-NLRP3 axis [12, 17]. Because Dohuo is the primary acting drug of DHJSD and may be the drug that exerts the important therapeutic effect, we will look into the possible molecular mechanism of Dohuo in the treatment of IVDD.

The group has been able to show the pathological process of IVDD and the possible method of DHJSD treatment based on the molecular mechanisms of pyroptosis, immunity, and inflammation; however, they have not been able to precisely explain the immune and cellular processes that are involved [9, 11, 12]. Additionally, the immune cells and subtypes implicated in the NPCs in IVDD can be found using single-cell sequencing studies. Furthermore, by integrating network pharmacology technology with bioinformatic analysis, we will conduct a thorough and methodical examination of the drug's mechanism and effects [18]. We thoroughly elucidated the subpopulations of NPCs and immune cells involved in the formation of IVDD using machine learning in conjunction with single-cell analysis. Subsequent enrichment studies helped to clarify the underlying molecular pathways linked to IVDD [19]. Lastly, in order to offer recommendations for the clinical management of IVDD, we employed network pharmacology to clarify the molecular mechanism of apoptosis in the dopamine treatment of IVDD.

2 | Materials and Methods

2.1 | Transcriptome Analysis Using Bioinformatics

2.1.1 | Analysis of Differential Genes

The NCBI Gene Expression Database provided bioinformatic data for intervertebral disc degeneration, of which GSE124272 data were chosen. The data sequencing platform for GPL21185 was Agilent-072363 SurePrint G3 Human GE v3 8×60K Microarray 039494 [Probe Name Version] [20]. The Gene ID Transformation tool in Sangerbox 3.0 was used to transform microarray matrix data to gene name matrix expression data. The R package Rtsne (version 0.15) was used for the investigation. Specifically, we ran a dimensionality reduction analysis using the Rtsne function to get a reduced matrix to look at the sample data after running a z-score on the expression spectrum [21]. The "limma" tool was then used for the purpose of identifying genes that differed between IVDD samples and normal control samples using differential gene analysis. Positive numbers indicate that differentially expressed genes (DEGs) are upregulated. The thresholds for differentially expressed genes were set at 1.2-fold and P.value < 0.05. In a similar vein, a 1.2-fold multiplicity of differences and a P.value < 0.05 indicate that genes with differential expression are down-regulated [21].

2.1.2 | Gene Screening for IVDD Hubs

Using the search term "intervertebral disk degeneration," genes associated with IVDD were found in the GeneCards database.

When the genes in the GeneCards database and the differentially expressed genes crossed paths, it was determined that the intersected genes were associated with the IVDD process [22]. Cytoscape software (version 3.9.1) was used to create the PPI network after the collected intersecting genes were analyzed using the string database (http://string-db.org/). The species restriction was set to "*Homo sapiens*" with a confidence value > 0.4 [23]. Furthermore, the intersecting gene regulatory network was constructed using the CytoHubba algorithm, a plug-in for Cytoscape software, and the top 20 important genes were selected based on the CytoHubba algorithm's Degree value ranking [24, 25]. In the string database, hub genes were examined for co-expression. Afterward, statistically significant hub genes were further screened for further investigation using differential violin plots.

2.1.3 | Analysis of Bioinformatic Process Enrichment

The intersecting genes were loaded into the oebiotech online data platform for bioinformatic process enrichment analysis, with the species restricted to "*H. sapiens*," in order to identify the pertinent signaling pathways and mechanisms of action of IVDD. Once the gene set's Gene Symbol was input into the common parameters and submitted, the results were shown in several graphs.

2.1.4 | Recognition of Immune Cells

The percentage of six different immune cell types (DC, NK, B, macrophage, neutrophil, and monocyte cells) as well as the fraction of 18 T cells can be estimated by immune cell AI. Additionally, it may forecast how well a patient would respond to immune checkpoint inhibitor medication and, in cases where group data are available, use conventional ANOVA testing to assess variations in the relative quantities of distinct immune cells among groups [26]. Using the transcriptome dataset, we employed the Immune Cell AI algorithm in the BioBean (Sheng-Xin-Dou-Ya-Cai) software to determine the immune cell types of patients with varying immunological patterns. The immune cell composition of the patients was then displayed using stacked graphs [27]. To find the immune cell infiltration correlations, correlation point bar graphs were constructed. At last, the distribution of immune cell data was shown and contrasted using Ridgeline plots, which are essentially overlapping combinations of numerous nuclear density profiles.

2.2 | Analysis of a Single Cell

2.2.1 | Data Processing Using a Single Cell

GPL24676 was used to create the scRNA-seq dataset GSE244889, which was obtained from the GEO database. In the NP tissue of mildly degenerative disc disease (MDD) and moderately severe degenerative disc disease (SDD), samples were taken for gene expression profiling at the single-cell level of NPCs. The data processing was carried out through the BioBean (Sheng-Xin-Dou-Ya-Cai) Analysis Tool, which

computes the mitochondrial content and rRNA content using the Percentage Feature Set function in the seurat package of the R language. It then performs a correlation analysis to determine the relationship between the mitochondrial content and the ncount (UMI) and the nFeature (number of genes). Based on the QC data, cell filtration criteria were established. The percentage of mitochondrial content was adjusted to 15% for features 6000 and below. pc number 15, along with the tsne/UMAP plot of the cell distribution in each sample following cell filtration, the cells were scattered and outliers in the tissues, necessitating further processing by the de-batch effect, which we performed using the harmonics de-batch this time [28].

2.2.2 | Annotations in Cells

We employed 2000 highly variable genes to reduce dimensionality using Principal Component Analysis (PCA). Using Seurat's Stochastic Neighbor Embedding (t-SNE) approach and the "FindNeighbors" and "FindClusters" (resolution = 0.1) functions, the best clusters were then chosen for display. Findmarker was utilized to filter subgroups of marker genes by comparing the expression levels of the top 5 (Top5) expressed genes; the higher the ranking, the greater the expression. Top5 marker genes, the "SingleR" package, the Human Protein Atlas, and a combination of literature searches were used to annotate various cell subpopulations and identify distinct cell types [29–31]. To illustrate the alterations in NP tissues' cellular profiles throughout the degeneration process, the quantity and percentage of cells in the sample for each cell subtype were also computed and displayed in two distinct bar charts.

2.2.3 | Cell Trajectory Analysis

Using the Monocle software tool (version 2.3.0), the differentiation trajectory analysis of NPCs was carried out to describe the relationships between the different NPCs subtypes. To facilitate temporal analysis, each sample's NPCs were separately removed and assembled into a Seurat object. The concept of "pseudo time" is introduced by the Monocle algorithm, which employs the individual cell sorting strategy. This method uses the variations in individual cell expression to sort all cells in accordance with a track, simulating the dynamic process of development or differentiation over time [32]. By comparing the pseudotimes of each individual NPCs subtype, the hierarchy of NPCs differentiation based on expression profiles was ascertained. The DDR Tress reduce Dimension function was utilized to determine the pseudotimes of various NPC isoforms, and then the trajectory graph was utilized to see the ensuing outcomes.

2.2.4 | Analysis of Cell-To-Cell Communication

To elucidate the cellular communication between NPC subtypes and immune cells, we applied the Cell Chat (version:1.6.1) algorithm to the scRNA-seq profiles of the various degeneration grades in the analysis of NP single-cell

transcriptome data from the same patient with varying degrees of degeneration. With the use of network analysis and pattern recognition techniques, Cell chat is a tool that makes it possible to quantitatively infer and analyze intercellular communication networks from scRNA-seq data. It does this by forecasting the main signaling inputs and outputs of a cell as well as how these cells and signals coordinate their activities. Based on the expression of intercellular ligands and receptors, Cell chat evaluates the significance of intercellular interactions. We focused on the apparent variations in cellular ligand/receptor interactions in cellular communication between different classes of samples to study the crucial function of cellular ligand/receptor interactions in IVDD [33].

2.2.5 | Combining Transcriptome Analysis With Single-Cell and Gene-Overlapping Analysis

The hub genes and IVDD intersection genes were acquired using general transcriptome sequencing, and they were examined alongside single-cell marker genes to confirm the relevant genes' expression patterns and biological mechanisms in various cells. To understand the expression of linked genes in various cells, R language packages were used to create UMAP maps of specific gene expression and particular gene expression violin maps.

2.3 | Analysis of the Mechanism of IVDD Treatment by Dohuo

2.3.1 | Screening of Blood-Entering Components of Duhuo

The majority of Traditional Chinese Medicines' (TCM) constituents are only able to have pharmacological effects once they have entered the bloodstream. These "components detected in the blood" comprise both the original TCM components that are directly absorbed into the bloodstream and their "metabolites," which are created by the liver and gastrointestinal system. The extraction of blood constituents from TCM is crucial for understanding their effectiveness, composition, and molecular mechanism. It also aids in the identification of absorbable and active lead compounds that are extracted from these TCM. The first systematic collection of blood constituents of TCM formulae and herbs is the Database of Constituents Absorbed into Blood and Metabolites of Traditional Chinese Medicine (DCABM-TCM), which was utilized in this work to gather the active ingredients in Duhuo (Radix Angelicae Biseratae) [34]. Natural products Magnetic Resonance Database, or NP-MRD, is a central repository for all NMR data produced by the natural goods industry. NP-MRD is going to be a web-enabled, FAIR-compliant, open-access database that holds structural and NMR spectrum data for every known natural product. With the help of the electronically available NP-MRD database, anyone can freely share and utilize vital data regarding the natural products found around the world. After collection, spectral data and chemical structures of the components that make up lone blood are queried in NP-MRD to confirm the accuracy of the compounds and to get ready for further analysis [35].

2.3.2 | Targets of Action of the Blood-Entering Component of Duhuo

For the only active blood entry components, the targets matching to the active compounds were gathered using the TCMSP, Swisstargetprediction database. The enrichment analysis was carried out based on the drug targets of the blood-entry components after the targets of the acquired compounds intersected with the intersecting targets of IVDD. Ultimately, the visualization linkage between "Duhuo-blood-entry component-target protein-signaling pathway-IVDD" was built using Cytoscape 3.9.1. It became clearer how Dohuo treats IVDD at the molecular level.

2.3.3 | Molecular Docking of Incoming Blood Components to Key Targets

The prior research provided the essential blood-entry components and useful targets for Duhuo (Radix Angelicae Biseratae)'s treatment of IVDD, but additional verification is required to confirm this prediction. In order to prove the drug's mechanism of action, the molecular docking technique can first show how well the active ingredient binds to the target proteins. After obtaining the 3D structure of the suggested docking target in mol2 format from the Pubchem database, AutodockTools 1.5.6 was used to open, process, and save the tiny ligand molecules as pdbqt files. As the docking protein, the target protein's core 3D structure from the RCSB protein database (www.rcsb.org/) was obtained. Save as pdbqt file after processing in AutodockTools 1.5.6. Ascertain the Vina molecule docking's coordinates and box size, set the parameter exhaustiveness to 15, and use the default values for the remaining parameters. For semi-flexible docking, Autodockvina 1.1.2 was utilized, and the optimal affinity conformation was chosen as the final docked conformation.

2.4 | Statistical Analysis

Plots and statistical analysis were done with Graphpad Prism 9.0. For results from three or more separate experiments, data were presented as histograms of mean $\pm$ standard error (SEM) values. If the samples fit into a normal distribution, a t-test was used to compare the two groups; if not, a non-parametric test was employed. ANOVA, or one-way analysis of variance, was employed to compare the samples from various groups. Every two groups were compared using Tukey's method test, where a difference of $p < 0.05$ indicated a statistically significant difference and $p < 0.01$ indicated a statistically significant difference.

3 | Results

3.1 | Results of Differential Gene Analysis

The GEO data were used to collect IVDD-related microarray data. Dimensionality reduction analysis revealed that the IVDD and normal group samples in the data were significantly separated in various places, indicating a dependable
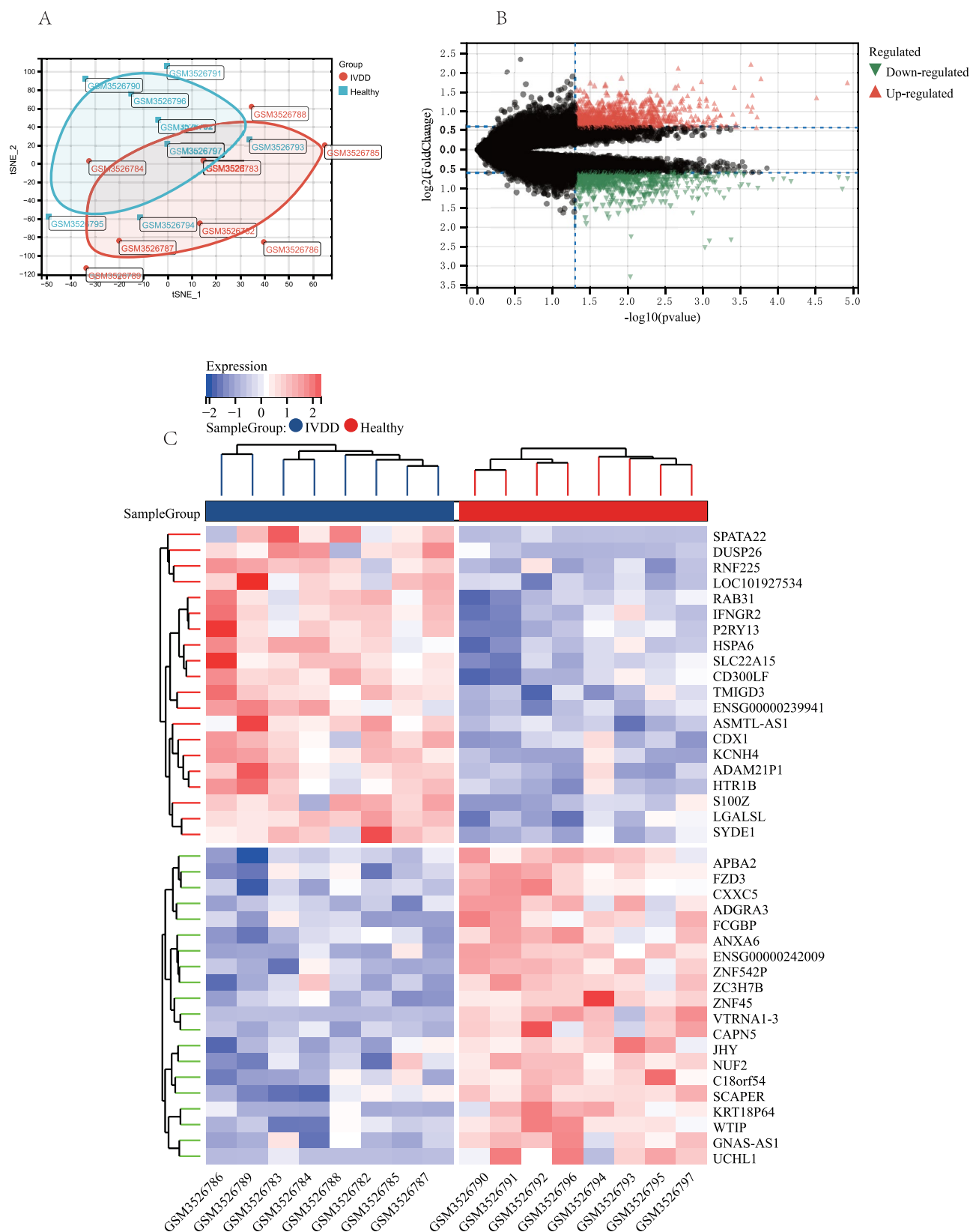
FIGURE 1 | Differential gene analysis: (A). Downscaling analysis of GSE124272 sample data, (B). Differential volcano plot of GSE124272 sample data, and (C). Differential heat map of GSE124272 sample data.

sample arrangement (Figure 1A). By using ID transformation, the IVDD dataset was generated (Table S1). Out of 29 381 genes, a differential analysis of the dataset identified 3741 DEGs, with 1466 genes exhibiting up-regulated expression and 2275 genes exhibiting down-regulated expression (Figure 1B,C, Table 1, Table S2).

TABLE 1 | Differential gene expression statistics for different differential ploidy.

Significance thresholds	Comparison group	Control group	1.2-fold difference		1.3-fold difference		1.5-fold difference		2-fold difference	
			Up	Down	Up	Down	Up	Down	Up	Down
$p < 0.05$	IVDD	Healthy	1466	2275	1268	1724	776	766	182	120
$p < 0.01$			422	616	383	503	268	262	83	61
FDR < 0.05			0	0	0	0	0	0	0	0
FDR < 0.01			0	0	0	0	0	0	0	0

3.2 | Results of the Hub Gene Screening

We were able to identify 933 IVDD disease-associated targets using the Genecard database (Table S3). A total of 143 intersecting genes were found by taking the Genecard data and comparing it with IVDD differential genes (Figure 2A, Table S4). These genes interacted, according to the PPI network, and additional Degree value sorting was done to identify the top 20 crucial genes (Figure 2B,C). TP53, JUN, HIF1A, PTEN, IL1B, ERBB2, IGF1, PARP1, SMAD3, MAPK8, CASP9, MET, TLR4, AR, PTK2, SOD2, EZH2, CCNB1, and TNFRSF1A were the 20 key genes. The results of the co-expression study demonstrated the strong interactions between the genes STAT3, TP53, JUN, HIF1A, PTEN, IL1B, ERBB2, IGF1, PARP1, SMAD3, MAPK8, CASP9, MET, TLR4, PTK2, SOD2, EZH2, and CCNB1 (Figure 2D). These genes were found to be differently expressed in IVDD by statistical analysis of variance; among these, TP53, JUN, PTEN, IL1B, ERBB2, MAPK8, CASP9, MET, TLR4, PTK2, SOD2, EZH2, and TNFRSF1A were statistically significant (*$p < 0.05$) (Figure 3, Table S5).

3.3 | Results of the Biological Process Enrichment Analysis

A total of 2149 GO terms were found to be enriched after we conducted enrichment analysis on 143 intersecting genes. These entries included 1545 biological process (BP), 257 cellular component (CC), and 347 molecular function (MF) entries (Table S6). Figure 4A,B displays chord diagrams and bar charts featuring the top 10 enrichment results in BP, CC, and MF. The findings indicate that the immunological response, NK cascade, positive regulation of gene expression, positive regulation of cytokine production involved in inflammatory response, skeletal system development, positive regulation of interleukin-6 production, cellular response to mechanical stimulus, vascular endothelial growth factor production, signal transduction in response to DNA damage, and inflammatory response are the primary focus of BP analysis in the IVDD process. CC is primarily positioned in the membrane, Golgi membrane, extracellular region, chromosome, telomeric region, basolateral plasma membrane, endoplasmic reticulum membrane, cell surface, extracellular space, site of double-strand break, plasma membrane MF Main Impact enzyme binding, identical protein binding, ATP binding, protein kinase binding, ubiquitin protein ligase binding, protein phosphatase binding, transmembrane signaling receptor activity, protein serine/threonine kinase binding, transcription coactivator binding, and RNA polymerase II-specific DNA-binding transcription factor binding. Two-hundred and thirty six signaling pathways are expressed throughout the IVDD process, according to KEGG pathway analysis (Table S7), and screening indicated that the majority of cellular processes are apoptosis, p53 signaling pathway. Environmental Information Processing mainly related to TNF signaling pathway, human diseases mainly included Lipid and atherosclerosis, Measles, Yersinia infection, Endocrine resistance, EGFR tyrosine kinase inhibitor resistance, Fluid shear stress and atherosclerosis, Kaposi sarcoma-associated herpesvirus infection, Central carbon metabolism in cancer, and Pathogenic *Escherichia coli* infection (Figure 4C,D). In conclusion, GO enrichment analysis demonstrated a strong correlation between the development of IVDD and cell immune response, inflammatory factor expression, and cell response to mechanical stimuli. Numerous studies also found a strong correlation between these findings and the cellular molecular mechanism of IVDD. In contrast, KEGG analysis mostly indicates a close relationship between the development of IVDD and the apoptosis of cells (Figure 4E).

3.4 | Results of Immune Infiltration Analysis

The Immune Cell AI algorithm was utilized to determine the IVDD immune infiltration score. The resulting immune infiltration score is displayed in a stacked graph (Table S8). The immune infiltration stack diagram revealed that Th1, Th2, Th17, Tfh, DC, B cell, monocyte, macrophage, NK, and other 24 immune cells were the primary immune cells engaged in IVDD (Figure 5A). Different immune cell infiltration correlations were shown by correlation dot bar graphs: CD4_T, CD4_naïve, Gamma_delta, Effector_memory, iTreg, Central memory, etc. displayed negative correlations, while monocytes, macrophages, neutrophils, DC, and so on showed positive correlations (Figure 5B). The immune cell distribution data is finally plotted in a mountain range plot, which compares and illustrates the differences in the graphical trends of B cells, monocytes, NK cells, CD4 naïve cells, and macrophages between the IVDD and normal groups (Figure 5C). These differences indicate that the immune cells significantly infiltrate the IVDD group and contribute to the development of disease.

3.5 | Cell Clustering

The expression matrix data were imported into the R software, and the R package Seurat was used to provide the necessary quality control to the data obtained from the NP tissues. We eliminated the cells that had more than 15% mitochondrial content after screening the cells with nFeature_RNA between 100
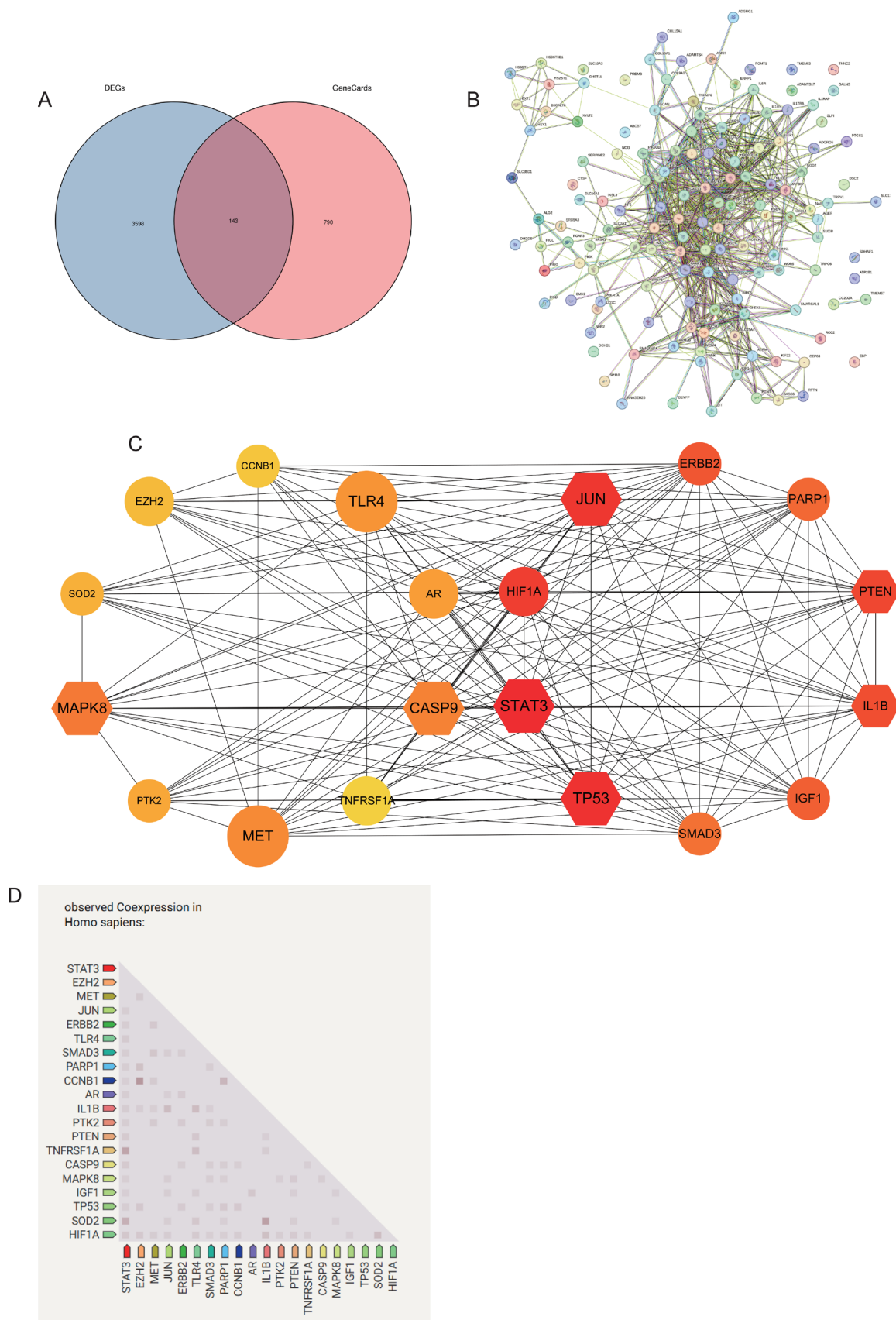
FIGURE 2 | Intersecting genes screening: (A). Intersecting Veen plot of Genecard data of IVDD with differential genes, (B). PPI network plot of intersecting genes, (C). Network plot of pivotal genes, and (D). Co-expression analysis of pivotal genes.
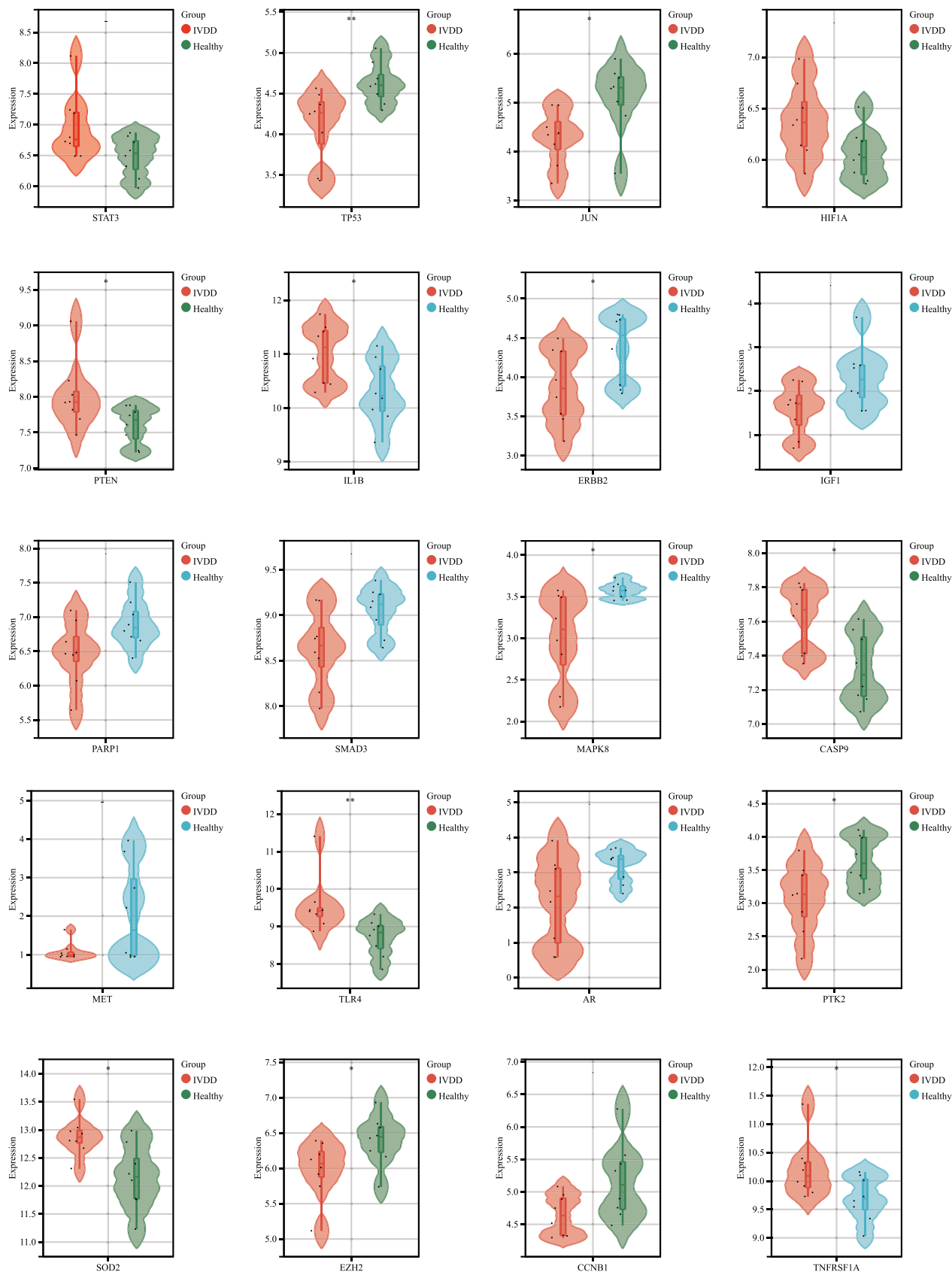
FIGURE 3 | Differential statistical violin plot for hub genes.

and 6000 and nCount_RNA count below 50000 (Figure 6A). In the meantime, the vst approach was used to identify the top 2000 highly variable genes for further downscaling and

grouping (Figure 6 B). ScRNA-seq composite data were acquired for NP samples with varying degrees of degeneration after thorough screening and batch effect correction analysis
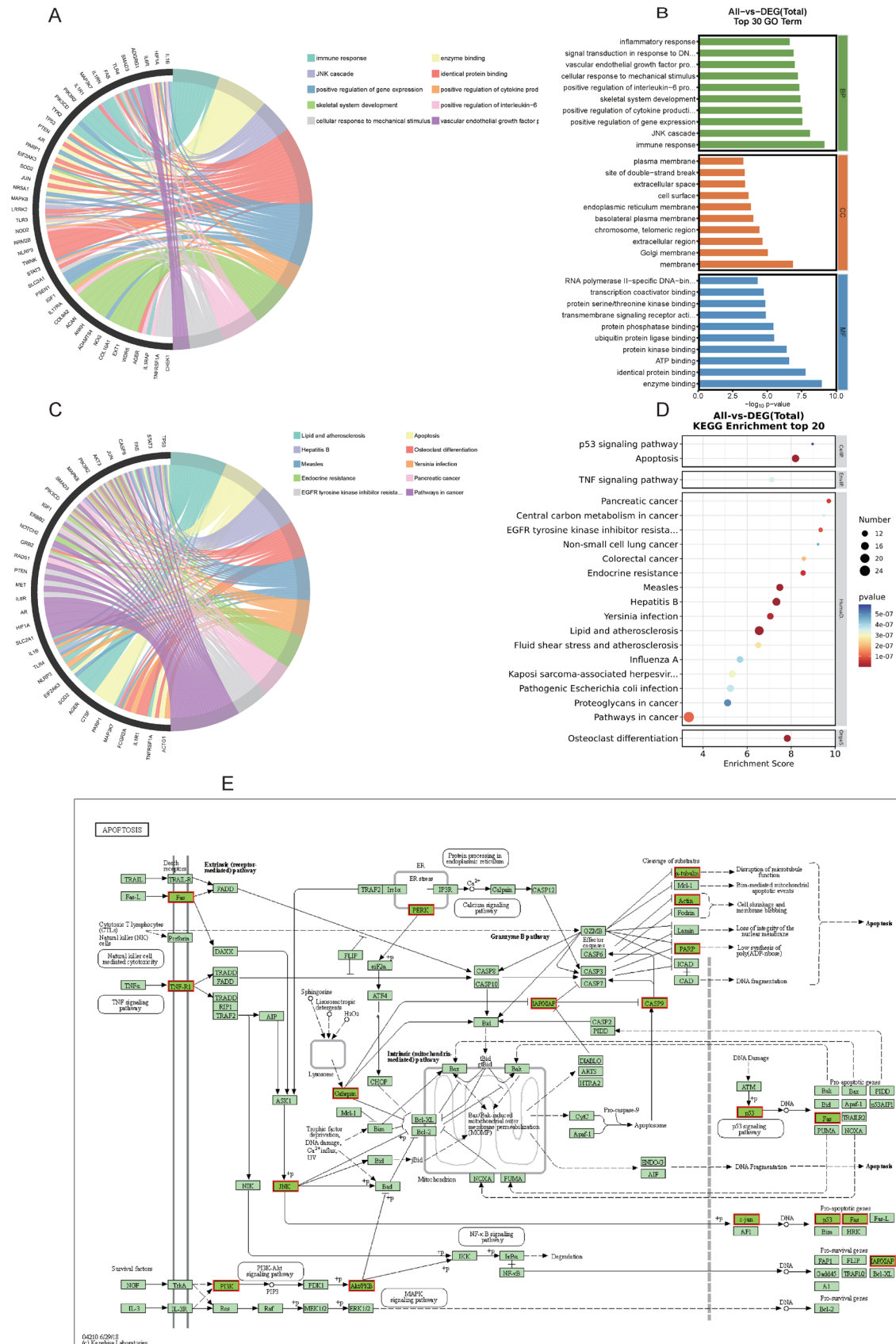
FIGURE 4 | Enrichment analysis: (A). GO enrichment analysis and chordal graph of intersecting genes, (B). GO enrichment analysis histogram of intersecting genes, (C). KEGG enrichment analysis and chordal graph of intersecting genes, (D). KEGG enrichment analysis and histogram of intersecting genes, and (E). Apoptosis signaling pathway and key proteins.
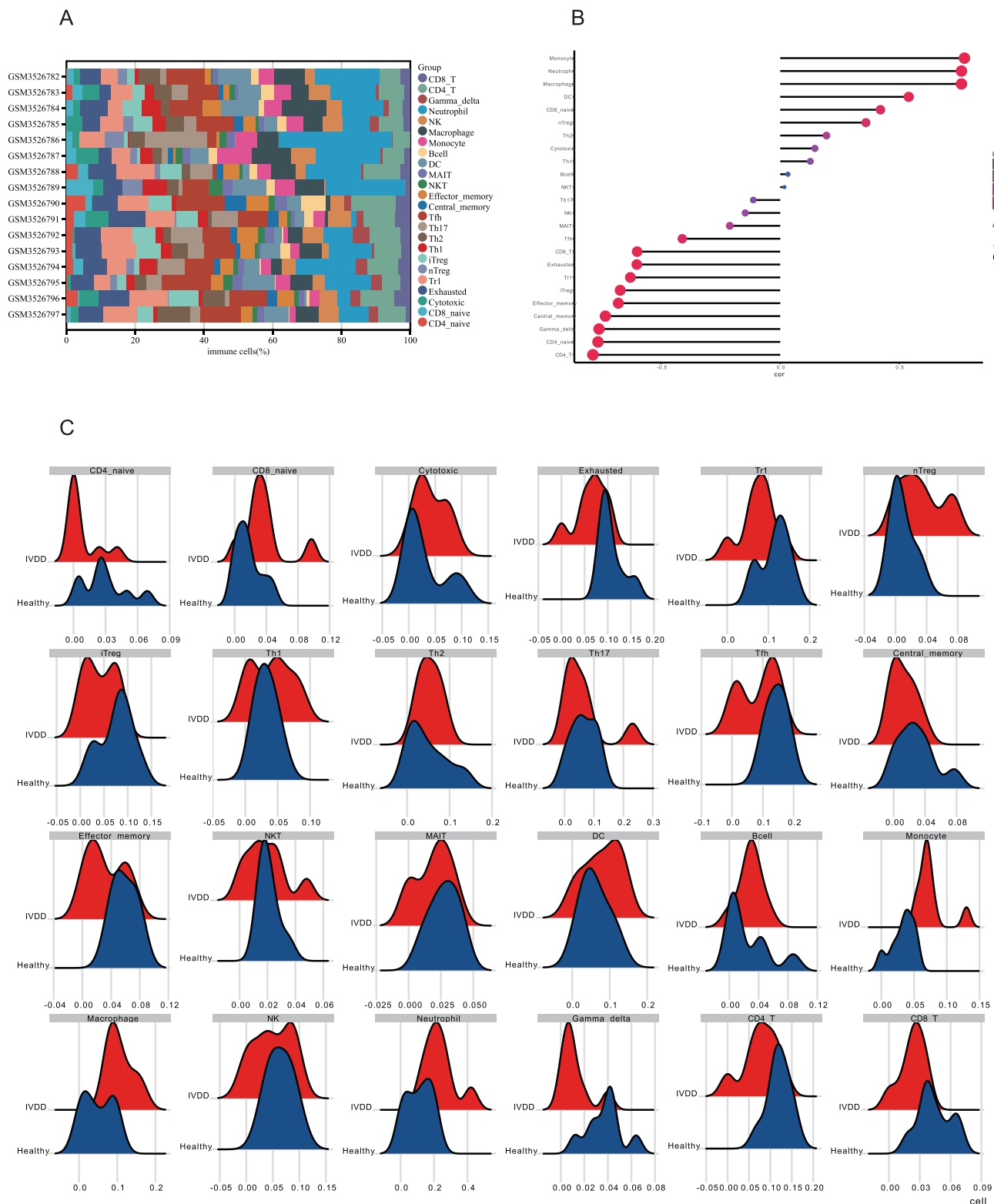
FIGURE 5 | Immune infiltration analysis: (A). Immune infiltration stacked plot, (B). Immune infiltration correlation dot bar graph, and (C). Immune infiltration mountain range plot.

of various data using the Harmony program (Figure 6C). After that, 11 unsupervised clusters were found using unsupervised UMAP cluster analysis (Figure 6D). The distribution map of the marker gene axis displays the distinctive genes of various subpopulations (Figure 6E). By means of a literature search, the singleR package for subpopulations, and marker genes,

we established annotations for 11 distinct cell populations (Figure 6F, Table S9). According to the NP cell classical markers, ACAN and SOX9, cell subtypes 0–3,10 were classified as NPCs and cell subtypes 4–9 as immune cells. NPCs were further refined and classified into 0 hypertrophic chondrocyte-like NPCs (HT-CL NPCs), one fibroNPCs, two adhesion NPCs,
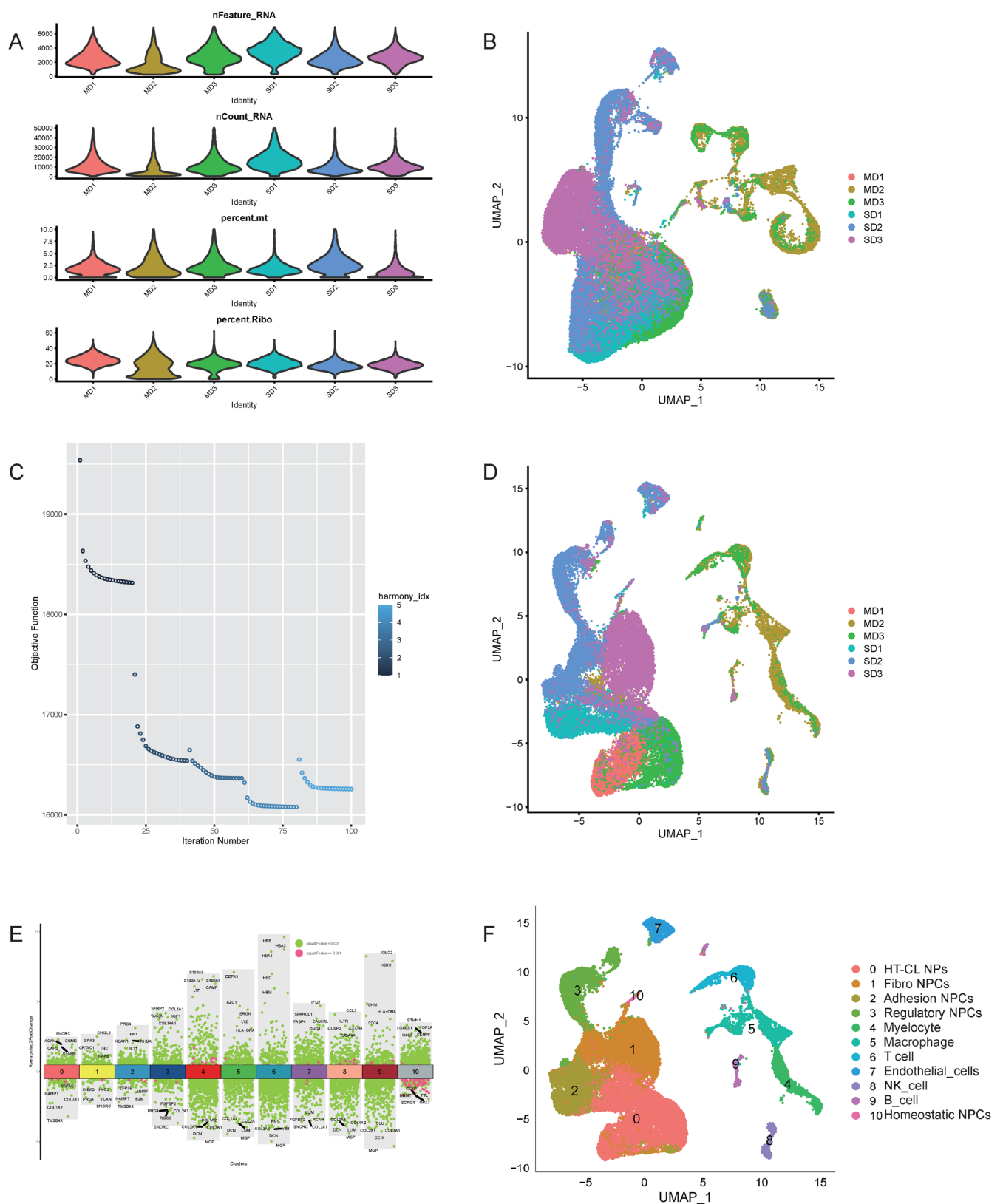
FIGURE 6 | Single-cell clustering: (A). Number of genes (nFeature_RNA), total number of UMIs (nCount_RNA), and percentage of mitochondrial gene expression (percent.mt), (B). Single-cell UMAP plots prior to de-batching, (C). HARMONY de-batching quality control, (D). UMAP distributions of the different sample tissues after removal of batches, (E). Marker gene axis distribution plot, and (F). Cell clustering distribution UMAP plot.

three regulatory NPCs, 10 homeostatic NPCs. Immune cells are further categorized into Myelocyte, Macrophage, T cell, Endothelial_cells, NK_cell, and B_cell. As demonstrated

by Figure 6D,F, immune cells were predominantly found in NP tissues that had mild degeneration, fibroNPCs, adhesion NPCs, regulatory NPCs, and homeostatic NPCs were

primarily found in NP tissues that had severe degeneration, and HT-CL NPCs were expressed in both mild and severe NP tissues.

3.6 | Cell Trajectory and Communication Analysis

The five NP cell subtypes were identified by matching their pseudotimes to determine the differentiation order. This allowed us to extract each NP cell separately and use the Monocle software package to analyze the NP cell differentiation trajectories in order to systematically simulate NP cell differentiation trajectories (Figure 7A). These cells are divided into nine future cell states by branch points 1, 2, 3, and 4, as shown in Figure 7B,C. The distribution of the 5 NP cell subtypes along the differentiation trajectory is shown in detail in Figure 7C,D. According to the data, fibroNPCs primarily appear in states 4 and 5, which represent the tail of the pseudotemporal differentiation, whereas the majority of adhesion NPCs appear in state 1, which is the start of the pseudotemporal differentiation and suggests that this NP cell is relatively high stemness. In addition, HT-CL NPCs display a bipolar distribution on the differentiation trajectory, with a small proportion at the beginning and a significant proportion at the tail of the trajectory. We used the Cell Chat algorithm to probe cellular communication in NP samples with varying degrees of degeneration because our single-cell sequencing data included NP tissue samples with varying grades of degeneration. This allowed us to identify changes in intercellular ligand/receptor interactions during degeneration. The figure illustrates that the intercellular communication in the highly degenerated NP tissues was considerably higher than in the mildly degenerated tissues. Additionally, the presence of immune cells in the mildly degenerated tissues implies that the early stages of degeneration, when immune cells were first introduced into the NPs, changed the cellular communication in the original NPs (Figure 7E,F). Further illustrates the expression of communication between every cell type and its neighboring cells. Ultimately, it was discovered that the MIF signaling pathway network had expanded as a result of the inclusion of immune cells such eight NK cells, nine B cells, and five macrophages. The primary targets of the signaling pathway were adhesion NPCs, fibroNPCs, homeostatic NPCs, and HT-CL NPCs. In these pathways, the most significant ligand/receptor interactions were CD74-ACKR3, CD74-CXCR4, and CD74-CD44. Thus, our initial theory was that the addition of immune cells like macrophages and NK cells to NP tissues that were deteriorating would trigger the MIF signaling pathway network, resulting in the slow development of NP cell adhesion, hypertrophy, fibrosis, and other pathological progression.

3.7 | Results of Combined Transcriptome and Single-Cell Analysis

Eleven co-analyzed genes were found by combining the intersection of IVDD transcriptome analysis of intersecting genes, hub genes, and single-cell marker gene intersection analysis. PPI analysis also demonstrated the interactions between these genes (Figure 8A,B). The distribution of cell subpopulations in the heatmap throughout the samples revealed that immune cells, particularly macrophages, T cells, B cells, monocytes, and NK cells, were the main infiltrators of the mildly deteriorated NP tissues. The most commonly seen NPC types in the highly deteriorated NP tissues were fibroNPCs, adhesion NPCs, regulatory NPCs, and homeostatic NPCs (Figure 8C). Eleven important genes linked to the progression of IVDD were additionally examined using transcriptome and single-cell analysis. PTEN, HIF1A, STAT3, IGF1, PARP1, SOD2, EZH2, JUN, and CCNB1 were shown to be highly distributed in various subpopulations, according to a UMAP map analysis of particular gene expression (Figure 8D–N). Consistent with the findings of cellular communication, further violin distribution maps based on these 11 hub genes revealed that these genes mostly regulate HT-CL NPCs, fibroNPCs, adhesion NPCs, homeostatic NPCs, and regulatory NPCs (Figure 8O).

3.8 | Mechanism of IVDD Treatment by Dohuo

The team's initial findings indicate that DHJSD is a traditional treatment for IVDD, with Duhuo serving as the key ingredient and monarch medication. Consequently, we examined Duhuo, a native Chinese medicinal herb from Sichuan, for its major blood-entering ingredients.

The major blood-entry components of Duhuo include Osthole, Columbianadin, Bergapten, Umbelliferone, Psoralen, Nodakenetin, Methoxsalen, Isoimperatorin, Imperatorin, columbianetin acetate, and Bergaptol (Figure 9A, Table 2). The photoplethysmograms of these constituents—Isoimperatorin, Imperatorin, Nodakenetin, and Methoxsalen—were further confirmed by NP-MRD. We also listed the molecular structures of these four compounds, which were not queried in the mass spectrometry data database (Figure 10). We gathered 537 Dohuo action targets using TCMSP and Swisstargetprediction, and we then took the intersection with the transcriptome intersection dataset to derive 19 therapeutic targets. We discovered that Dohuo might enhance IVDD by engaging in apoptosis, the ErbB signaling route, the FoxO signaling pathway, and the HIF-1 signaling pathway, based on the KEGG enrichment analysis of the 19 therapeutic targets (Figure 9B). Ultimately, the developed network pharmacological molecular mechanism map demonstrated that Duhuo worked in concert with multiple targets, multiple components, and multiple pathways to enhance IVDD (Figure 9C).

3.9 | Results of Molecular Docking

We have established that the active components of Dohuo improve IVDD by enhancing NPC apoptosis, based on the enrichment analysis of the entry components and major action targets of Dohuo. Additionally, we discovered that the primary ingredients of Duhuo, Osthole, Columbianadin, and Bergapten might function by influencing apoptosis through the primary targets of CASP9, MAPK8, PTGS1, and PARP1. The molecular docking studies additionally confirmed the ability of Osthole, Bergapten, and Columbianadin to bind to the important targets (Figure 11, Table 3).
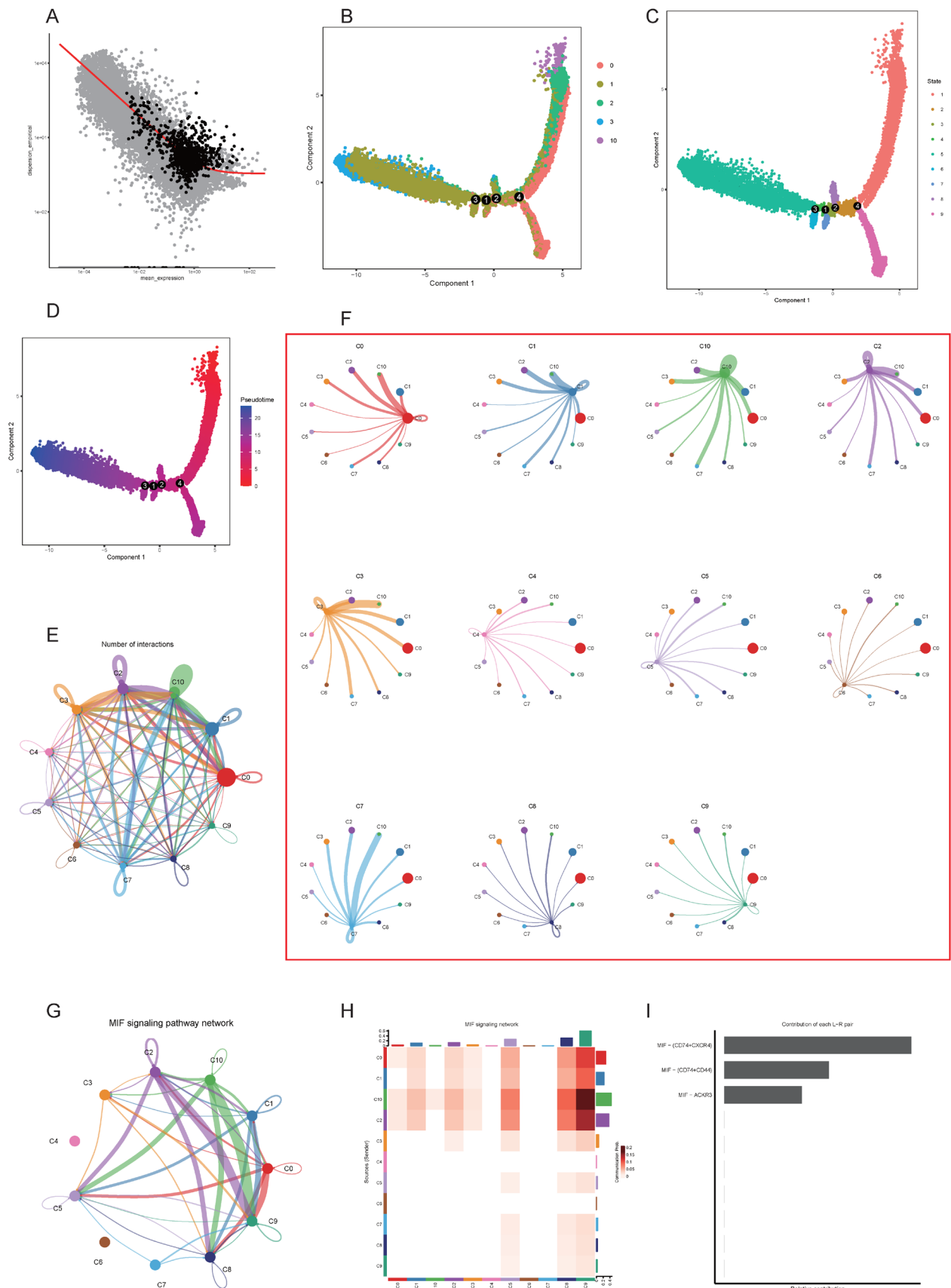
FIGURE 7 | Cell trajectory and communication analysis: (A). Scatter plot of 1,2,3,10 cell subpopulation trajectory analysis, (B). 1,2,3,10 cell subpopulation trajectory composition, (C). 1,2,3,10 cell subpopulation trajectory differentiation status, (D). 1,2,3,10 cell subpopulation trajectory temporal status, (E). Summary of cell subpopulation communication, (F). Expression of communication of every cell subpopulation with other cells, (G). MIF signaling pathway network expression in different subpopulations, (H). Heatmap of MIF signaling pathway network expression in different subpopulations, and (I). Receptor ligands of the MIF signaling pathway network.
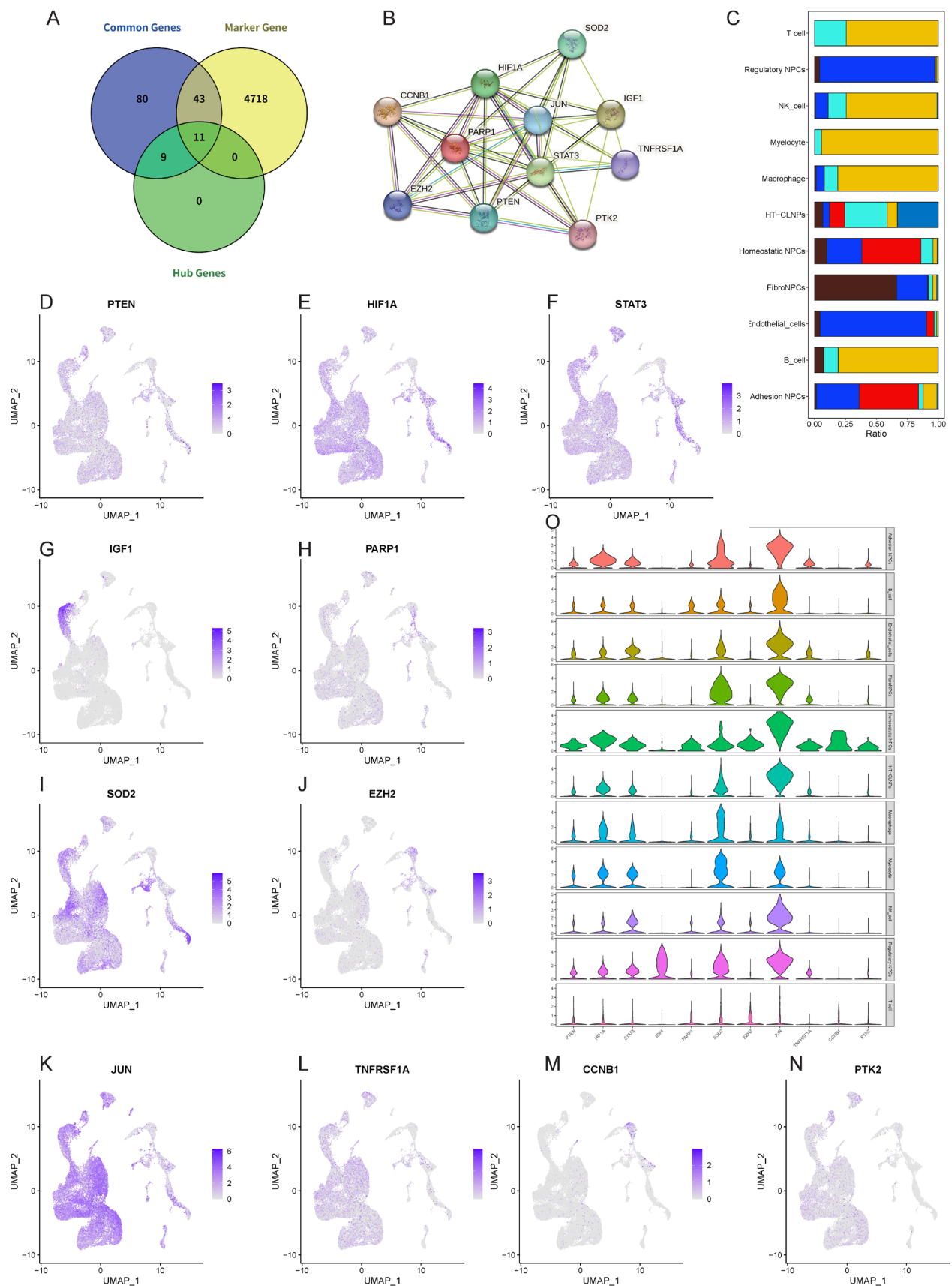
FIGURE 8 | Co-analysis: (A). IVDD transcriptome analysis of intersecting genes, hub genes, and single-cell marker genes intersection analysis, (B). PPI network map of 11 genes in the co-analysis, (C). Distribution heatmap of cellular subpopulations in different samples, (D–N): UMAP distribution of the 11 genes in the co-analysis, and (O). Violin map of the 11 genes in the co-analysis.
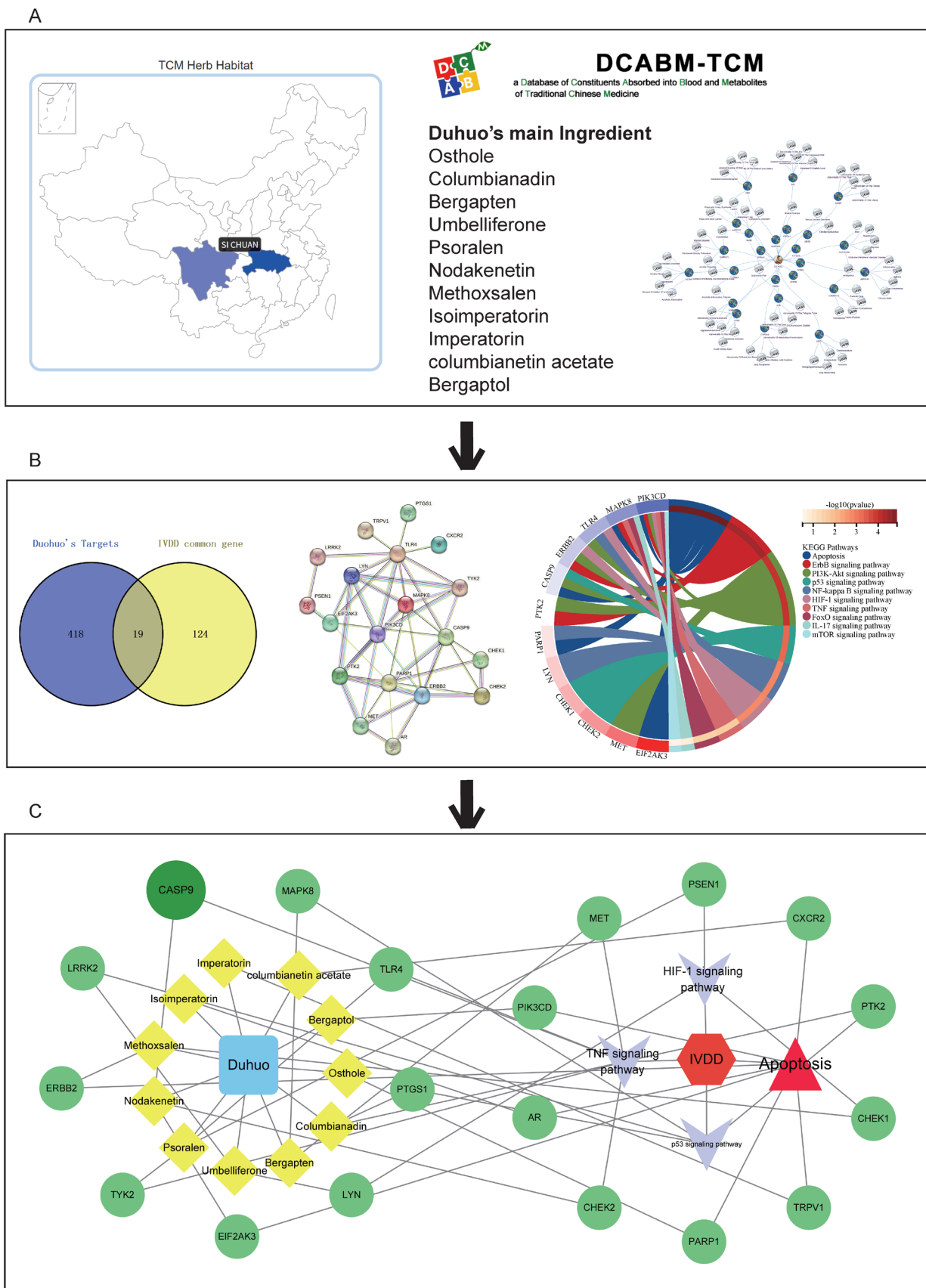
FIGURE 9 | Mechanism of IVDD treatment by Duhuo.

TABLE 2 | The blood-entering component of Duhuo.

Compound name	Chemical formula	Pubchem CID	DCABM ID
Osthole	C15H16O3	10 228	BC209_S
Columbianetin(no target)	C14H14O4	92 201	BC2738_S
Columbianadin	C19H20O5	6 436 246	BC70_S
Bergapten	C12H8O4	2355	BC1414_S
Umbelliferone	C9H6O3	5 281 426	BC2631_S
Psoralen	C11H6O3	6199	BC1436_S
Oxypeucedanin hydrate(no target)	C16H16O6	17 536	BC1394_S
Nodakenetin	C14H14O4	26 305	BC1975_S
Methoxsalen	C12H8O4	4114	BC1546_S
Meranzin hydrate(no target)	C15H18O5	5 070 783	BC2715_S
Isoimperatorin	C16H14O4	68 081	BC2028_S
Imperatorin	C16H14O4	10 212	BC2678_S
Columbianetin acetate	C16H16O5	161 409	BC364_S
Bergaptol	C11H6O4	5 280 371	BC3466_S
Angelol b(no target)	C20H24O7	10 022 392	BC1924_S

4 | Discussion

Inflammation, oxidative stress, and NPC death are the primary pathogenic processes of IVDD, the most common lumbar spine illness affecting middle-aged and older adults globally [36]. There are many different cells that contribute to the formation of IVDD. Immune cells primarily consist of monocytes, macrophages, T-cells, B-cells, and neutrophils, whereas pathogenic process cells primarily consist of ECM degradation, NPC senescence, apoptosis, etc. [37]. The study of tumor heterogeneity, immunological microenvironment cell differentiation, and other scientific topics has made extensive use of single-cell sequencing technology, a new technology with promising development possibilities [28, 38]. An increasing number of researchers have been using scRNA-seq technologies to study the pathophysiological network mechanisms underlying IVDD and its development in recent years [39]. Due to its osmotic qualities and abundance of type II collagen (COL2) and proteoglycans (ACAN), the NP, one of the most important parts of the IVD, is essential to the physiological function of the disc. It also helps to maintain the height and compressive strength of the NP by retaining more fluid. As a result, we primarily decided to investigate NP's modifications in IVDD as the subject of our study.

We have discovered pivotal genes, including TP53, JUN, PTEN, IL1B, ERBB2, MAPK8, CASP9, MET, TLR4, PTK2, SOD2, EZH2, TNFRSF1A, and others, through machine learning. These genes' molecular mechanisms primarily relate to immune response, inflammatory factor expression, cellular response to mechanical stimuli, and apoptosis. Immunoassays showed that CD4-naïve, B cell, monocyte, NK, and macrophage development were closely related to IVDD development. The present single-cell mapping found

five subpopulations of NPCs, including HT-CL NPCs, fibroNPCs, adhesion NPCs, regulatory NPCs, and homeostatic NPCs. Immune cell subpopulations consist of monocyte, macrophage, T cells, endothelial cells, NK cells, and B cells. HT-CL NPCs were expressed in both mild and severe NP tissues, whereas fibroNPCs, adhesion NPCs, regulatory NPCs, and homeostatic NPCs were primarily found in the tissues of extensively degraded NP. The majority of immune cells were found in NP tissues that had mild degeneration. While the results of our research are similar to those of Tu J and his team's single-cell resolution transcriptional profile of human NP, which also identifies new human NP cell subtypes, our analysis's results are also more credible [40]. The most common cell subtypes in NPs according to our study were fibroNPCs, adhesion NPCs, regulatory NPCs, and homeostatic NPCs. As NP degradation progressed, these cell subtypes' numbers and proportions grew noticeably. These cells were primarily enriched in the signaling pathways of inflammation, immunity, hypoxia, and apoptosis, according to a further examination of their biological functions. This suggests that these cells are the main NP cell subtypes that cause degeneration and that they are involved in the pathophysiological mechanism of IVDD.

The primary cause of IVDD has long been understood to be inflammation, and degenerative disc tissues exhibit markedly elevated expression of cellular pro-inflammatory molecules such TNF-α and IL-1β. Inflammatory mediators such as TNF-α and IL-1β generated enhanced cellular inflammatory response and accelerated NP cell senescence and death during disc degradation. A vicious cycle of NP damage and degeneration will result from discs under prolonged inflammatory load, which will attract chemokines and inflammatory substances once more and exacerbate NP cell destruction [9, 11]. The maintenance of immunological homeostasis by a variety
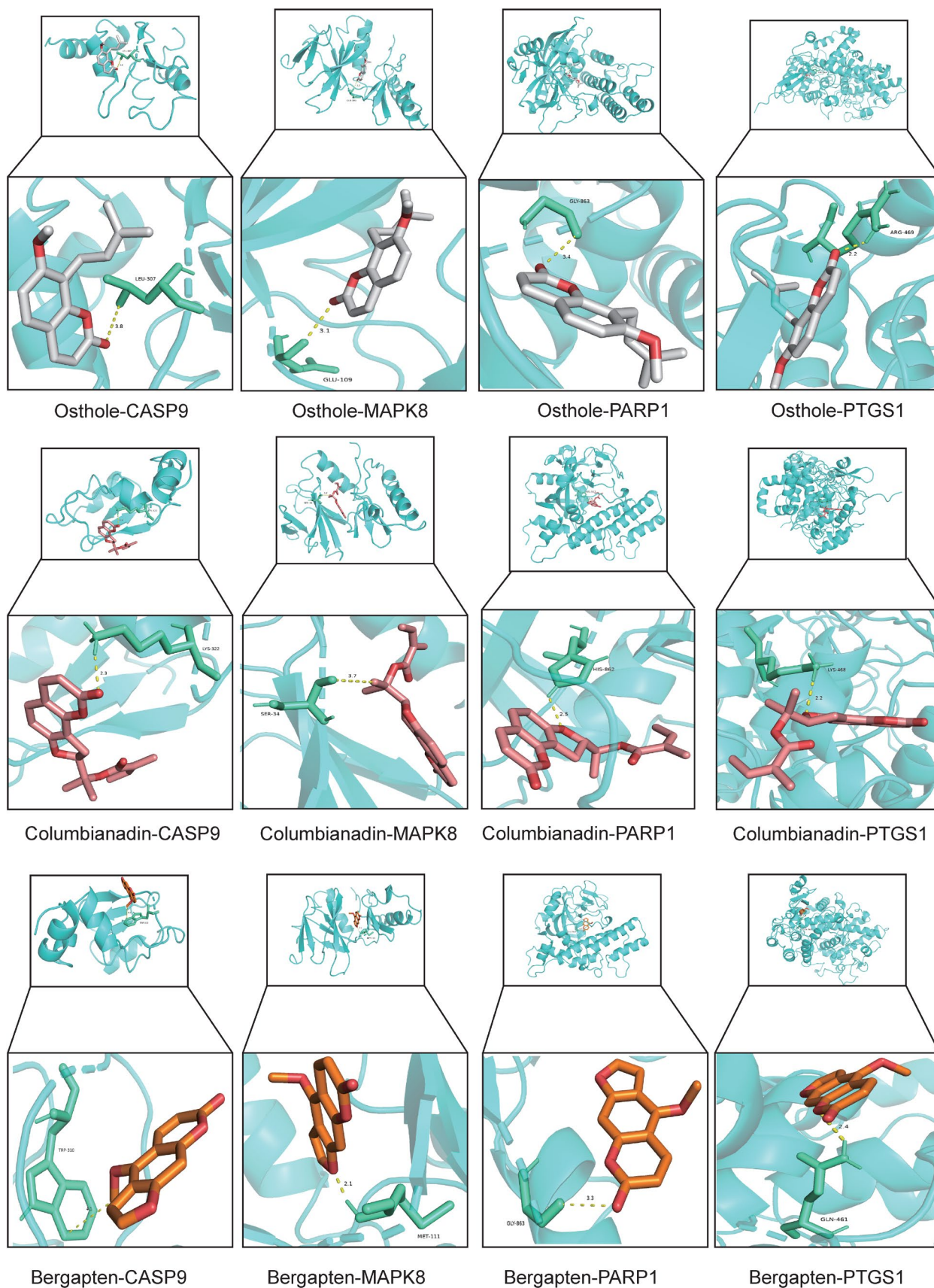
FIGURE 10 | Mass spectrometry data of the main blood entry components of Duhuo.

FIGURE 11 | Molecular docking results.

TABLE 3 | The binding energy of molecular docking (kJ mol).

Hub genes active chemicals	CASP9	MAPK8	PARP1	PTGS1
Osthole	−5.0	−7.9	−8.7	−7.3
Columbianadin	−6.0	−9.9	−11.6	−6.6
Bergapten	−4.7	−7.3	−7.4	−7.2

of immune cells, such as mast cells, macrophages, T and B cells, and others, is essential to the IVD process. Macrophages in the IVDD process have garnered a lot of interest lately. Human NP and endplate disc degeneration is positively connected with levels of macrophage markers, these correlations are higher in cadaveric specimens that exhibit unhealthy regions of impaired disc structure [41]. It was shown that the polarization of macrophages had distinct roles in the course of IVDD. M1 macrophages exacerbated the suppression of cell proliferation and IVD degeneration, whereas M2 macrophages moderated the development of IVDD [42]. Furthermore, multiprotein complexes of innate immune receptors and sensors known as inflammatory vesicles stimulate caspase-dependent inflammation and apoptosis. Although it has been observed that other cell types can also trigger inflammasome activation, macrophages and other innate immune cells are the primary source of inflammasome activation. Thus, based on the findings of our investigation, we hypothesize that macrophages can trigger inflammatory vesicles and proteins essential for apoptosis, namely CASP9, which causes NPCs to undergo apoptosis and aggravates IVDD.

Even while nonsteroidal anti-inflammatory medicines (NSAIDs) and corticosteroids, which are currently used to treat IVDD, are helpful, they come with a lot of negative effects. In this sense, natural substances possessing strong anti-inflammatory and antioxidant qualities could be a valuable asset for the creation of IVDD treatments. The team discovered that DHJSD contains antioxidant, scavenges ROS, and controls NPCs death [43]. As a result, this time we looked into the mechanism of action of its primary medication, Duhuo. The primary active ingredients in Dihuo are Osthole, Columbianadin, Bergapten, Umbelliferone, Psoralen, Nodakenetin, Methoxsalen, Isoimperatorin, Imperatorin, Columbianetin Acetate, and Bergaptol, according to our research of blood entry components. We gathered the Dohuo targets using TCMSP and Swisstargetprediction, intersected them with the transcriptome intersection dataset once more, and produced 19 therapeutic targets. By using KEGG enrichment analysis, we were able to determine that Duhuo can enhance IVDD by increasing its involvement in the following signaling pathways: Apoptosis, ErbB, FoxO, and HIF-1.

Although Duhuo has not been extensively studied in IVDD, we think that it can ameliorate IVDD by controlling NPC apoptosis via key genes such CASP9, MAPK8, PTGS1, PARP1, etc. To sum up, our investigation revealed that IVDD is caused by the infiltration of several immune cells, including B cells, T cells, NK cells, macrophages, and myelocytes, which cause NPCs to undergo apoptosis. The blood-entry components of Douhuo,

osthole, Columbianadin, and Bergapten are naturally occurring substances that can bind to CASP9, MAPK8, PTGS1, and PARP1 in the center, mediate NPC apoptosis and inflammation, and so prevent NPC death and lessen IVDD. Numerous fruits and herbs contain the furanocoumarin phytohormone bergapten, which has anti-inflammatory properties. Through the promotion of mitochondrial autophagy and preservation of mitochondrial homeostasis, Bergapten inhibited NLRP3 inflammatory vesicle activation and pyroptosis in a study that characterized the therapeutic potential of the compound for bacterial infections and inflammation-related diseases and clarified the underlying mechanisms. Based on these findings, it appears that Bergapten holds promise as a therapy for disorders associated with inflammation [44]. Another study discovered that the ANP32A/ATM signaling pathway is activated by bergapten to produce its anti-inflammatory properties [45]. The anti-inflammatory and anti-apoptotic mechanisms of the relevant drugs will be further validated by in vitro experiments in forthcoming studies, as these substances have not been extensively explored in IVDD.

5 | Conclusion

In conclusion, it was discovered that immune cell infiltration, particularly that of macrophages, T cells, and monocyte cells, and numerous subtype alterations of NPCs are strongly associated with the development of IVDD. NPC apoptosis is largely influenced by CASP9, MAPK8, PTGS1, and PARP1. Osthole, Columbianadin, and Bergapten, the active blood entry component, may enhance IVDD by controlling these essential proteins to prevent NPC apoptosis.

References

1. J. Dowdell, M. Erwin, T. Choma, A. Vaccaro, J. Iatridis, and S. K. Cho, "Intervertebral Disk Degeneration and Repair," *Neurosurgery* 80, no. 3s (2017): S46–s54.

2. N. D. Jeffery, J. M. Levine, N. J. Olby, and V. M. Stein, "Intervertebral Disk Degeneration in Dogs: Consequences, Diagnosis, Treatment, and Future Directions," *Journal of Veterinary Internal Medicine* 27, no. 6 (2013): 1318–1333.

3. C. K. Kepler, D. G. Anderson, C. Tannoury, and R. K. Ponnappan, "Intervertebral Disk Degeneration and Emerging Biologic Treatments," *Journal of the American Academy of Orthopaedic Surgeons* 19, no. 9 (2011): 543–553.

4. J. Zhao, J. Wang, H. Xu, et al., "Intervertebral Disk Degeneration and Bone Mineral Density: A Bidirectional Mendelian Randomization Study," *Calcified Tissue International* 114, no. 3 (2024): 228–236.

5. I. Han, A. E. Ropper, D. Konya, et al., "Biological Approaches to Treating Intervertebral Disk Degeneration: Devising Stem Cell Therapies," *Cell Transplantation* 24, no. 11 (2015): 2197–2208.

6. P. P. Raj, "Intervertebral Disc: Anatomy-Physiology-Pathophysiology-Treatment," *Pain Practice* 8, no. 1 (2008): 18–44.

7. E. González Martínez, J. García-Cosamalón, I. Cosamalón-Gan, M. Esteban Blanco, O. García-Suarez, and J. A. Vega, "Biology and Mechanobiology of the Intervertebral Disc," *Neurocirugía (Asturias, Spain)* 28, no. 3 (2017): 135–140.

8. L. J. Smith, N. L. Nerurkar, K. S. Choi, B. D. Harfe, and D. M. Elliott, "Degeneration and Regeneration of the Intervertebral Disc: Lessons From Development," *Disease Models & Mechanisms* 4, no. 1 (2011): 31–41.

9. C. Song, Y. Zhou, K. Cheng, et al., "Cellular Senescence - Molecular Mechanisms of Intervertebral Disc Degeneration From an Immune Perspective," *Biomedicine & Pharmacotherapy* 162 (2023): 114711.

10. C. Song, Y. Xu, Q. Peng, et al., "Mitochondrial Dysfunction: A New Molecular Mechanism of Intervertebral Disc Degeneration," *Inflammation Research* 72, no. 12 (2023): 2249–2260.

11. C. Song, W. Cai, F. Liu, K. Cheng, D. Guo, and Z. Liu, "An In-Depth Analysis of the Immunomodulatory Mechanisms of Intervertebral Disc Degeneration," *JOR Spine* 5, no. 4 (2022): e1233.

12. D. Guo, K. Cheng, C. Song, et al., "Mechanisms of Inhibition of Nucleus Pulposus Cells Pyroptosis Through SDF1/CXCR4-NFkB-NLRP3 Axis in the Treatment of Intervertebral Disc Degeneration by Duhuo Jisheng Decoction," *International Immunopharmacology* 124 (2023): 110844.

13. H. Li, X. Wang, H. Pan, et al., "The Mechanisms and Functions of IL-1β in Intervertebral Disc Degeneration," *Experimental Gerontology* 177 (2023): 112181.

14. Z. Wang, X. Hu, W. Wang, et al., "Understanding Necroptosis and Its Therapeutic Target for Intervertebral Disc Degeneration," *International Immunopharmacology* 121 (2023): 110400.

15. L. Lu, J. Hu, Q. Wu, et al., "Berberine Prevents Human Nucleus Pulposus Cells From IL-1β-Induced Extracellular Matrix Degradation and Apoptosis by Inhibiting the NF-κB Pathway," *International Journal of Molecular Medicine* 43, no. 4 (2019): 1679–1686.

16. C. Song, R. Chen, K. Cheng, et al., "Exploring the Pharmacological Mechanism of Duhuo Jisheng Decoction in Treating Intervertebral Disc Degeneration Based on Network Pharmacology," *Medicine (Baltimore)* 102, no. 22 (2023): e33917.

17. P. Cazzanelli and K. Wuertz-Kozak, "MicroRNAs in Intervertebral Disc Degeneration, Apoptosis, Inflammation, and Mechanobiology," *International Journal of Molecular Sciences* 21, no. 10 (2020): 3601.

18. F. Chen, L. Lei, S. Chen, et al., "Serglycin Secreted by Late-Stage Nucleus Pulposus Cells Is a Biomarker of Intervertebral Disc Degeneration," *Nature Communications* 15, no. 1 (2024): 47.

19. Y. Zhao, Y. Mu, Y. Zou, et al., "Integrated Analysis of Single-Cell Transcriptome and Structural Biology Approach Reveals the Dynamics Changes of NP Subtypes and Roles of Menaquinone in Attenuating Intervertebral Disc Degeneration," *Journal of Biomolecular Structure & Dynamics* 42 (2023): 1–24.

20. Q. Xiang, Y. Zhao, and W. Li, "Identification and Validation of Ferroptosis-Related Gene Signature in Intervertebral Disc Degeneration," *Front Endocrinol (Lausanne)* 14 (2023): 1089796.

21. X. Xiong, C. Chen, X. Li, et al., "Identification of a Novel Defined Inflammation-Related Long Noncoding RNA Signature Contributes to Predicting Prognosis and Distinction Between the Cold and Hot Tumors in Bladder Cancer," *Frontiers in Oncology* 13 (2023): 972558.

22. S. Huang, "Efficient Analysis of Toxicity and Mechanisms of Environmental Pollutants With Network Toxicology and Molecular Docking Strategy: Acetyl Tributyl Citrate as an Example," *Sci Total Environ* 905 (2023): 167904.

23. C. Zhao and S. Sahni, "String Correction Using the Damerau-Levenshtein Distance," *BMC Bioinformatics* 20, no. Suppl 11 (2019): 277.

24. X. Q. Lu, J. Q. Zhang, S. X. Zhang, et al., "Identification of Novel Hub Genes Associated With Gastric Cancer Using Integrated Bioinformatics Analysis," *BMC Cancer* 21, no. 1 (2021): 697.

25. H. Dong, X. Li, M. Cai, et al., "Integrated Bioinformatic Analysis Reveals the Underlying Molecular Mechanism of and Potential Drugs for Pulmonary Arterial Hypertension," *Aging (Albany NY)* 13, no. 10 (2021): 14234–14257.

26. K. E. Craven, Y. Gökmen-Polar, and S. S. Badve, "CIBERSORT Analysis of TCGA and METABRIC Identifies Subgroups With Better Outcomes in Triple Negative Breast Cancer," *Scientific Reports* 11, no. 1 (2021): 4691.

27. J. I. Kawada, S. Takeuchi, H. Imai, et al., "Immune Cell Infiltration Landscapes in Pediatric Acute Myocarditis Analyzed by CIBERSORT," *Journal of Cardiology* 77, no. 2 (2021): 174–178.

28. T. Stuart and R. Satija, "Integrative Single-Cell Analysis," *Nature Reviews. Genetics* 20, no. 5 (2019): 257–272.

29. M. Massimino, F. Martorana, S. Stella, et al., "Single-Cell Analysis in the Omics Era," *Technologies and Applications in Cancer, Genes (Basel)* 14, no. 7 (2023): 1330.

30. D. Zucha, M. Kubista, and L. Valihrach, "Tutorial: Guidelines for Single-Cell RT-qPCR," *Cells* 10, no. 10 (2021): 2607.

31. T. L. Lee, "Single Cell Genomics," *International Journal of Biochemistry & Cell Biology* 116 (2019): 105596.

32. Z. Ren, P. Yu, D. Li, et al., "Single-Cell Reconstruction of Progression Trajectory Reveals Intervention Principles in Pathological Cardiac Hypertrophy," *Circulation* 141, no. 21 (2020): 1704–1719.

33. S. Jin, C. F. Guerrero-Juarez, L. Zhang, et al., "Inference and Analysis of Cell-Cell Communication Using CellChat," *Nature Communications* 12, no. 1 (2021): 1088.

34. X. Liu, J. Liu, B. Fu, et al., "DCABM-TCM: A Database of Constituents Absorbed Into the Blood and Metabolites of Traditional Chinese Medicine," *Journal of Chemical Information and Modeling* 63, no. 15 (2023): 4948–4959.

35. D. S. Wishart, Z. Sayeeda, Z. Budinski, et al., "NP-MRD: The Natural Products Magnetic Resonance Database," *Nucleic Acids Research* 50, no. D1 (2022): D665–d677.

36. S. M. Rider, S. Mizuno, and J. D. Kang, "Molecular Mechanisms of Intervertebral Disc Degeneration," *Spine Surg Relat Res* 3, no. 1 (2019): 1–11.

37. Y. Wang, H. Cheng, T. Wang, K. Zhang, Y. Zhang, and X. Kang, "Oxidative Stress in Intervertebral Disc Degeneration: Molecular Mechanisms, Pathogenesis and Treatment," *Cell Proliferation* 56, no. 9 (2023): e13448.

38. N. Slavov, "Single-Cell Protein Analysis by Mass Spectrometry," *Current Opinion in Chemical Biology* 60 (2021): 1–9.

39. Z. Lu and Z. Zheng, "Integrated Analysis of Single-Cell and Bulk RNA Sequencing Data Identifies the Characteristics of Ferroptosis in Lumbar Disc Herniation," *Functional & Integrative Genomics* 23, no. 3 (2023): 289.

40. J. Tu, W. Li, S. Yang, et al., "Single-Cell Transcriptome Profiling Reveals Multicellular Ecosystem of Nucleus Pulposus During Degeneration Progression," *Single-Cell Transcriptome Profiling Reveals Multicellular Ecosystem of Nucleus Pulposus During Degeneration Progression, Adv Sci (Weinh)* 9, no. 3 (2022): e2103631.

41. J. Koroth, E. O. Buko, R. Abbott, et al., "Macrophages and Intervertebral Disc Degeneration," *International Journal of Molecular Sciences* 24, no. 2 (2023): 1367.

42. X. C. Li, S. J. Luo, W. Fan, et al., "Macrophage Polarization Regulates Intervertebral Disc Degeneration by Modulating Cell Proliferation, Inflammation Mediator Secretion, and Extracellular Matrix Metabolism," *Frontiers in Immunology* 13 (2022): 922173.

43. S. H. Lim, H. S. Lee, H. K. Han, and C. I. Choi, "Saikosaponin A and D Inhibit Adipogenesis via the AMPK and MAPK Signaling Pathways in 3T3-L1 Adipocytes," *International Journal of Molecular Sciences* 22, no. 21 (2021): 11409.

44. T. Luo, X. Jia, W. D. Feng, et al., "Bergapten Inhibits NLRP3 Inflammasome Activation and Pyroptosis via Promoting Mitophagy," *Acta Pharmacologica Sinica* 44, no. 9 (2023): 1867–1878.

45. Y. He, Z. Zisan, Z. Lu, L. Zheng, and J. Zhao, "Bergapten Alleviates Osteoarthritis by Regulating the ANP32A/ATM Signaling Pathway," *FEBS Open Bio* 9, no. 6 (2019): 1144–1152.

Supporting Information

Additional supporting information can be found online in the Supporting Information section.